

High Dispersion Spectroscopy of Solar-type Superflare Stars.

II. Stellar Rotation, Starspots, and Chromospheric Activities

Yuta NOTSU¹, Satoshi HONDA², Hiroyuki MAEHARA^{3,4}, Shota NOTSU¹, Takuya SHIBAYAMA⁵, Daisaku NOGAMI^{1,6}, and Kazunari SHIBATA⁶
ynotsu@kwasan.kyoto-u.ac.jp

¹*Department of Astronomy, Kyoto University, Kitashirakawa-Oiwake-cho, Sakyo-ku, Kyoto 606-8502*

²*Center for Astronomy, University of Hyogo, 407-2, Nishigaichi, Sayo-cho, Sayo, Hyogo 679-5313*

³*Kiso Observatory, Institute of Astronomy, School of Science, The University of Tokyo, 10762-30, Mitake, Kiso-machi, Kiso-gun, Nagano 397-0101*

⁴*Okayama Astrophysical Observatory, National Astronomical Observatory of Japan, 3037-5 Honjo, Kamogata, Asakuchi, Okayama 719-0232*

⁵*Solar-Terrestrial Environment Laboratory, Nagoya University, Furo-cho, Chikusa-ku, Nagoya, Aichi, 464-8601*

⁶*Kwasan and Hida Observatories, Kyoto University, Yamashina-ku, Kyoto 607-8471*

(Received 29-Sep-2014; accepted 26-Dec-2014)

Abstract

We conducted high dispersion spectroscopic observations of 50 superflare stars with Subaru/HDS. These 50 stars were selected from the solar-type superflare stars that we had discovered from the Kepler data. More than half (34 stars) of these 50 target superflare stars show no evidence of binarity, and we estimated stellar parameters of these 34 stars in our previous study (Notsu et al. 2015, hereafter called Paper I). According to our previous studies using Kepler data, superflare stars show quasi-periodic brightness variations whose amplitude (0.1-10%) is much larger than that of the solar brightness variations (0.01-0.1%) caused by the existence of sunspots on the rotating solar surface. In this study, we investigated whether these quasi-periodic brightness variations of superflare stars are explained by the rotation of a star with fairly large starspots, by using stellar parameters derived in Paper I. First, we confirmed that the value of the projected rotational velocity $v \sin i$ is consistent with the rotational velocity estimated from the period of the brightness variation. Next, we measured the intensity of Ca II infrared triplet lines and H α line, good indicators of the stellar chromospheric activity, and compared them with other stellar properties.

The intensity of Ca II infrared triplet lines indicates that the mean magnetic field strength ($\langle fB \rangle$) of the target superflare stars can be higher than that of the Sun. A correlation between the amplitude of the brightness variation and the intensity of Ca II triplet line was found. All the targets expected to have large starspots because of their large amplitude of the brightness variation show high chromospheric activities compared to the Sun. These results support that the brightness variation of superflare stars is due to the rotation with large starspots.

Key words: stars: flare — stars: solar-type — stars: rotation — stars: spots — stars: activity

1. Introduction

Flares are the energetic explosions in the stellar atmosphere and are thought to occur by intense releases of magnetic energy stored around starspots, like solar flares (e.g., Shibata & Magara 2011). The total energy released in the largest solar flares is estimated to be of the order of 10^{32} erg (e.g., Priest 1981; Emslie et al. 2012). Many “superflare” events have been recently found by using the Kepler data (Maehara et al. 2012; Shibayama et al. 2013). Superflares are gigantic flare events that are $10\text{--}10^6$ times more energetic ($\sim 10^{33\text{--}38}$ erg; Schaefer et al. 2000) than the largest solar flares on the Sun ($\sim 10^{32}$ erg). We have analyzed the data from Kepler space telescope (Koch et al. 2010), and discovered 365 superflare events on 148 solar-type (G-type main-sequence) stars from the data of 83,000 solar-type stars observed for the first 120 days of the Kepler mission (Maehara et al. 2012). We here define solar-type stars as the stars that have a surface temperature of $5100 \leq T_{\text{eff}} \leq 6000\text{K}$ and a surface gravity of $\log g \geq 4.0$. Extending the study of Maehara et al. (2012), we found 1547 superflare events on 279 solar-type stars by using the Kepler data of a longer period (~ 500 days) (Shibayama et al. 2013). Kepler is very useful for detecting small increases in the stellar brightness caused by stellar flares, because Kepler realized high photometric precision exceeding 0.01% for moderately bright stars, and obtained continuous time-series data of many stars over a long period (Koch et al. 2010).

The analyses of Kepler data enabled us to discuss statistical properties of superflares since a very large number of flare events were discovered. Shibayama et al. (2013) confirmed that the occurrence rate (dN/dE) of the superflare versus the flare energy (E) has a power-law distribution of $dN/dE \propto E^{-\alpha}$, where $\alpha \sim 2$, and this distribution is roughly similar to that for the solar flare. Shibayama et al. (2013) also estimated that a superflare with an energy of

10^{34-35} erg occurs once in 800-5000 years in Sun-like stars. “Sun-like stars” are here defined as solar-type stars with an effective temperature of $5600 \leq T_{\text{eff}} \leq 6000\text{K}$, a surface gravity of $\log g \geq 4.0$, and a rotation period (P) longer than 10 days.

Considering these results, we have performed more analyses in order to investigate whether properties of superflare stars can be explained by applying our current physical understanding of the Sun. Solar flares are the intense releases of magnetic energy stored around sunspots, as mentioned above. If we assume superflares are the similar magnetic energy releases, large starspots are necessary to explain their large amount of energy. Many of the superflare stars show quasi-periodic brightness variations with a typical period of from one day to a few tens of days. The amplitude of these brightness variations is in the range of 0.1-10% (Maehara et al. 2012), and is much larger than that of the solar brightness variation (0.01-0.1%; e.g., Lanza et al. 2003) caused by the existence of sunspots on the rotating solar surface. Many ordinary solar-type stars observed by Kepler also show such brightness variations and these variations are thought to be caused by the rotation of a star having starspots (e.g., Basri et al. 2011; Reinhold et al. 2013). Notsu et al. (2013b) showed that the above brightness variations of superflare stars can be well explained by the rotation of a star with fairly large starspots, taking into account the effects of inclination angle and the spot latitude. In other words, the existence of large starspots is also supported by the brightness variations.

Notsu et al. (2013b) compared the superflare energy and frequency with the rotation period, assuming that the brightness variation period corresponds to the rotation period. They then found slowly rotating stars can still produce as energetic flares as those of more rapidly rotating stars although the average flare frequency is lower for more slowly rotating stars. Notsu et al. (2013b) also clarified that the superflare energy is related to the total coverage of the starspots, and that the energy of superflares can be explained by the magnetic energy stored around these large starspots. In addition, Shibata et al. (2013) suggested, on the basis of theoretical estimates, that the Sun can generate large magnetic flux sufficient for causing superflares with an energy of 10^{34} erg within one solar cycle ($\sim 11\text{yr}$).

The results described above are, however, only based on Kepler monochromatic photometric data. We need to spectroscopically investigate whether these brightness variations are explained by the rotation, and whether superflare stars have large starspots. The stellar parameters and the binarity of the superflare stars are also needed to be investigated with spectroscopic observations in order to discuss whether the Sun can really generate superflares.

We have then performed high dispersion spectroscopy of 50 superflares stars. We have already reported some results of our spectroscopic observations of three superflare stars in

Notsu et al. (2013a) and Nogami et al. (2014). In particular, Nogami et al. (2014) found that spectroscopic properties (T_{eff} , $\log g$, $[\text{Fe}/\text{H}]$, and rotational velocity) of the two superflare stars KIC9766237 and KIC9944137 are very close to those of the Sun. In Notsu et al. (2015; hereinafter referred to as Paper I), we have already conducted measurements of stellar parameters for the sake of detailed discussions in this paper. In paper I, we investigated the binarity of the target stars, and found that more than half (34 stars) of 50 target superflare stars have no evidence of binarity. We then estimated temperature (T_{eff}), surface gravity ($\log g$), metallicity ($[\text{Fe}/\text{H}]$), and projected rotational velocity ($v \sin i$) of these 34 “single” superflare stars. The accuracy of our stellar atmospheric parameters (T_{eff} , $\log g$, and $[\text{Fe}/\text{H}]$) is higher than that of KIC (Kepler Input Catalog; Brown et al. 2011) values, and the differences between our values and KIC values ($(\Delta T_{\text{eff}})_{\text{rms}} \sim 219\text{K}$, $(\Delta \log g)_{\text{rms}} \sim 0.37$ dex, and $(\Delta [\text{Fe}/\text{H}])_{\text{rms}} \sim 0.46$ dex) are comparable to the large uncertainties and systematic differences in KIC values reported by the previous researches (e.g., Brown et al. 2011). We confirmed that the estimated temperature and $\log g$ values of these 34 superflare stars are roughly in the range of solar-type (G-type main sequence stars) stars. In particular, the temperature, surface gravity, and the brightness variation period (P_0) of 9 stars including two stars (KIC9766237 and KIC9944137) reported in Nogami et al. (2014) are in the range of “Sun-like” stars ($5600 \leq T_{\text{eff}} \leq 6000\text{K}$, $\log g \geq 4.0$, and $P_0 > 10$ days). We also found that five of the 34 target stars are fast rotators ($v \sin i \geq 10\text{km s}^{-1}$), while 22 stars have relatively low $v \sin i$ values ($v \sin i < 5\text{km s}^{-1}$). These results suggest that stars whose spectroscopic properties similar to the Sun can have superflares, and this supports the hypothesis that the Sun might cause a superflare.

On the basis of the above stellar parameters derived in Paper I, in this paper we investigate whether the brightness variation is explained by the rotation, and whether superflare stars have large starspots. In this process, we use “ $v \sin i$ ” estimated in Paper I. Moreover, we use the intensity of Ca II infrared triplet (Ca II IRT, $\lambda = 8498, 8542, 8662\text{\AA}$) lines and $\text{H}\alpha$ line, which we have already used for investigating chromospheric activity in Notsu et al. (2013a) and Nogami et al. (2014). Ca II IRT and $\text{H}\alpha$ lines are well-known good indicators of the chromospheric activity of G-type stars (e.g., Takeda et al. 2010; Soderblom et al. 1993b; Notsu et al. 2013a).

In Section 2, we briefly explain the observational data used in this paper. In Section 3.1, we show the measurement results of the intensity of Ca II IRT and $\text{H}\alpha$ lines. We then indirectly estimate the mean intensity of stellar magnetic field using Ca II 8542 line on the basis of our solar spectroheliographic observation in Section 3.2. In Section 4, we compare “ $v \sin i$ ” with the period of the brightness variation, and consider whether the brightness variation is explained by the rotation. In Section 5, we discuss stellar chromospheric activities, including the starspot sizes and rotational velocity of superflare stars.

2. Observational Data

The details of our spectroscopic observations are described in Section 2 of Paper I. Our observations have been performed by using the High Dispersion Spectrograph (HDS: Noguchi et al. 2002) at the 8.2-m Subaru telescope. The names of the above 34 superflare stars, which show no evidence of binarity in Paper I, and 10 comparison stars are shown in Table 1. In addition to the above 10 comparison stars, Moon was also observed as a comparison star in this observation, as briefly mentioned in Section 2.2 of Paper I. The observed spectra of these stars around Ca II 8542 and H α 6563 are shown in Figures 1 and 2, respectively. We did not use Ca II 8542 line of 7 target superflare stars (KIC7093547, KIC8359398, KIC8547383, KIC9459362, KIC10252382, KIC10387363, and KIC11818740) since the resultant S/N ratio around Ca II IRT lines is low, as we can see in Figure 1. We show these stars with a comment “low S/N” in this figure. Examples of spectra around photospheric lines, including Fe I 6212, 6215, 6216, 6219 are shown in Figure 3. As we have already mentioned in Paper I, we observed 13 superflare stars among these 34 superflare stars, and 3 comparison stars (59 Vir, 61 Vir, and 18 Sco) multiple times. We made co-added spectra of these 16 stars in total, which have “S12B-comb” or “S13A-comb” in Supplementary Table 2 of Paper I. In Figures 1, 2, and 3, co-added spectra of these 16 stars are used. Only the co-added spectra are used in this paper when we analyze the spectral data of these 16 stars.

3. Measurements of stellar activity indicators

3.1. Measurements of Ca II Infrared Triplet and H α

In order to investigate the chromospheric activity of the target stars, we measured $r_0(8498)$, $r_0(8542)$, $r_0(8662)$, and $r_0(\text{H}\alpha)$ index, which are the residual core flux normalized by the continuum level at the line cores of the Ca II IRT and H α , respectively. As we have already introduced previous researches in detail in Section 3.3 of Notsu et al. (2013a), these indexes are known to be good indicators of stellar chromospheric activity (e.g., Linsky et al. 1979; Takeda et al. 2010). As the chromospheric activity is enhanced, the intensity of these indicators becomes large since a greater amount of emission from the chromosphere fills in the core of the lines. The values of $r_0(8498)$, $r_0(8542)$, $r_0(8662)$, and $r_0(\text{H}\alpha)$ indexes of the target single superflare stars and comparison stars are listed in Table 1. We were not able to measure the values of Ca II IRT indexes ($r_0(8498)$, $r_0(8542)$, and $r_0(8662)$) of 7 target superflare stars (KIC7093547, KIC8359398, KIC8547383, KIC9459362, KIC10252382, KIC10387363,

and KIC11818740) because of low S/N ratios around Ca II IRT lines. For reference, we also measured the emission flux of Ca II IRT and H α lines in Appendix 1.

3.2. Indirect estimation of mean intensity of the stellar magnetic field using Ca II 8542 line.

As mentioned above, Ca II lines are good indicators of stellar chromospheric activity, and the intensity of them well correlates with the intensity of stellar magnetic field. Schrijver et al. (1989) derived a rough empirical relation between the emission core flux of Ca II K line and the average photospheric magnetic field, on the basis of spectroheliographic observations of solar active regions. In this paper, we extended this relation to the emission core flux of Ca II 8542 ($r_0(8542)$) and the average stellar magnetic field by newly carrying out spectroheliographic observations of solar active regions. We summarized the method and results in the following of this section.

In order to derive an empirical relation, we compared $r_0(8542)$ values obtained from spectroheliographic observation of the active region NOAA11654, with the photospheric magnetic field strength data of the same region on the same observation date. The spectroheliographic observation was conducted using 60cm Domeless Solar Telescope (DST) with the horizontal spectrograph of the Hida Observatory, Kyoto University (Nakai & Hattori 1985). The observation date was 2013 January 11th (JST). The photospheric magnetic field strength data ($\langle fB \rangle$; “ f ” is a filling factor) that we used here were taken by HMI (Scherrer et al. 2012; Schou et al. 2012) on the Solar Dynamics Observatory (SDO; Pesnell et al. 2012) on the same day.

Adjusting the spatial scale of both the DST and HMI data to $2''.4 \times 2''.4$, we plotted $r_0(8542)$ value of each data point in the target active region as a function of $\langle fB \rangle$ (mean intensity of the photospheric magnetic field) of the same point. As shown in Figure 4 (a), a rough positive correlation is seen between $r_0(8542)$ and $\langle fB \rangle$. This figure means that $r_0(8542)$ index roughly reflects the average intensity of the stellar magnetic field ($\langle fB \rangle$), though this correlation is not so good especially for less active stars (low $\langle fB \rangle$). Using the least-square method, we conduct a linear fit in the double logarithmic graph $\log r_0(8542)$ vs. $\log(\langle fB \rangle)$ (Figure 4 (b)). As a result, we derived a very rough empirical relation between $r_0(8542)$ and $\langle fB \rangle$:

$$\log r_0(8542) = -0.587 + 0.156 \times \log(\langle fB \rangle) . \quad (1)$$

We then roughly estimate $\langle fB \rangle$ values of the target stars, by using Equation (1) and $r_0(8542)$ values. The estimated $\langle fB \rangle$ values are listed in Table 1. The error value of each $\langle fB \rangle$ value in Table 1 is estimated from the standard deviation of $\langle fB \rangle$ distribution as a function of

$r_0(8542)$ in Figure 4. In addition, if we apply Equation (1) to solar $r_0(8542)$ value estimated in Takeda et al. (2010) ($r_0(8542)=0.193$), $\langle fB \rangle$ is estimated to be 0.2 ± 6 [Gauss]. This value is consistent with the values of solar mean magnetic field (a few Gauss) within its error range, though the error range is large.

4. Rotational Velocity and Inclination Angle

As mentioned above, we reported the values of projected rotational velocity ($v \sin i$), stellar radius (R_s), and the brightness variation period (P_0) of the 34 “single” target superflare stars in Paper I. The values of $v \sin i$ and P_0 are listed again in Table 1. Assuming that the brightness variations of these stars are caused by the rotation of the stars with starspots, we can estimate the rotational velocity (v_{lc}) from P_0 and R_s by using

$$v_{lc} = \frac{2\pi R_s}{P_0}, \quad (2)$$

as we have already mentioned in Section 5.2 of Notsu et al. (2013a). The resultant values of v_{lc} are listed in Table 1. We here consider that the typical error of v_{lc} is about $\pm 25\%$, assuming that the upper limit of errors of R_s and P_0 are about 20% and 10%, respectively, on the basis of Paper I.

In Figure 5, we plot $v \sin i$ as a function of the v_{lc} . Some data points in Figure 5 show differences between the values of v_{lc} and $v \sin i$. The projected rotational velocity ($v \sin i$) tends to be smaller than v_{lc} . Such differences should be explained by the inclination effect, as mentioned in the previous studies (e.g., Hirano et al. 2012; Notsu et al. 2013a). On the basis of $v \sin i$ and v_{lc} , the stellar inclination angle (i) can be estimated by using the following relation:

$$i = \arcsin\left(\frac{v \sin i}{v_{lc}}\right). \quad (3)$$

In Figure 5, we also show four lines indicating $i = 90^\circ$ ($v \sin i = v_{lc}$), $i = 60^\circ$, $i = 30^\circ$, and $i = 10^\circ$. This figure shows two following important results. First, for almost all the stars (33 stars) except for KIC11764567, the relation “ $v \sin i \lesssim v_{lc}$ ” is satisfied. This is consistent with our assumption that the brightness variation is caused by the rotation since the inclination effect mentioned above can cause the relation “ $v \sin i \lesssim v_{lc}$ ” if v_{lc} values really correspond to the rotational velocities (i.e. $v = v_{lc}$). This is also supported by another fact that the distribution of the data points in Figure 5 are not random. Their distribution is expected to be much more random if the brightness variations have no relations with the stellar rotation. Second, stars that are distributed in the lower right side of Figure 5 are expected to have small inclination angles and to be nearly pole-on stars. In this figure, we distinguish such five stars with especially small inclination angle ($i \leq 13^\circ$) (KIC3626094, KIC4742436, KIC6503434,

KIC6934317, and KIC9412514) from the other stars, using filled triangle data points.

We can confirm the above inclination effects from another point of view, as already mentioned for KIC6934317 in Figure 7 of Notsu et al. (2013a). Figure 6 is a scatter plot of the flare energy of superflares and solar flares as a function of the spot coverage. The data used in this figure are the same as in Figure 10 of Notsu et al. (2013b). The spot coverage of superflare stars are calculated from the amplitude of stellar brightness variations, and the energy of superflares are estimated by using the superflare amplitude and the duration time (Shibayama et al. 2013). Thick and thin solid lines correspond to the analytic relation between the spot coverage and the flare energy, which is obtained from Equation (14) of Notsu et al. (2013b) in case of $i = 90^\circ$ for $B=3,000\text{G}$ and $1,000\text{G}$. The thick and thin dashed lines correspond to the same relation in case of $i = 2^\circ$ (nearly pole-on) for $B=3,000\text{G}$ and $1,000\text{G}$, assuming that the brightness variation becomes small as a result of the inclination effect. These lines are considered to give an upper limit of superflare energy for each inclination angle (Notsu et al. 2013b). Considering these things, the superflare stars located in the upper left side of this figure are expected to have a low inclination angle. Open triangles in Figure 6 correspond to superflare stars whose inclination angle is especially small ($i \leq 13^\circ$) on the basis of Figure 5, while open circles represent the other stars ($i > 13^\circ$). This classification is the same as that in Figure 5. All of the five triangle data points are located above the thick solid line ($i = 90^\circ$ and $B=3000\text{G}$). This means that these stars are also confirmed to have low inclination angle on the basis of Figure 5. As a result, these two figures (Figure 5 and 6) are confirmed to be consistent, and in other words, the stellar projected rotational velocity spectroscopically measured is consistent with the rotational velocity estimated from the brightness variation. The fact indicates that the brightness variation of superflare stars is caused by the rotation.

5. Stellar Chromospheric Activity and Starspots of Superflare Stars

In Figure 7 (a), we plot $r_0(8542)$ as a function of T_{eff} of the target superflare stars. The data of ordinary solar-type stars reported in Takeda et al. (2010) are also plotted in this figure. The variability range of $r_0(8542)$ between the solar maximum and solar minimum is only $0.19 \sim 0.20$ (Livingston et al. 2007). This figure shows that almost all the target superflare stars are more active compared to the Sun from the viewpoint of the $r_0(8542)$ index. In other words, the mean magnetic field strength of the target stars can be higher than that of the Sun (see Section 3.2). In addition, 4 target superflare stars (KIC8429280, KIC9652680, KIC10528093, and KIC11610797) show much higher chromospheric activity ($r_0(8542) > 0.6$) compared to the other solar-type stars in this figure.

In Figure 7 (b), we plot $r_0(8542)$ as a function of $v \sin i$ of the target superflare stars. The data of ordinary solar-type stars reported in Takeda et al. (2010)¹ are also plotted for reference in this figure. There is a rough positive correlation between $r_0(8542)$ and $v \sin i$, and more rapidly rotating stars have higher chromospheric activity. All of the 5 stars with extremely high $v \sin i$ value ($v \sin i \geq 10 \text{ km s}^{-1}$) compared to the Sun ($v \sin i \sim 2 \text{ km s}^{-1}$) show relatively high $r_0(8542)$ values ($r_0(8542) \gtrsim 0.5$). This is consistent with many previous observational results of ordinary main-sequence stars (e.g., Noyes et al. 1984; Takeda et al. 2010). In addition, about 6 superflare stars with relatively small $v \sin i$ values ($v \sin i \lesssim 5 \text{ km s}^{-1}$) in this figure (KIC4831454, KIC6865484, KIC8802340, KIC11140181, KIC11303472, and KIC12266582) also have relatively high chromospheric activity ($r_0(8542) \gtrsim 0.5$) compared to the data of ordinary solar-type stars taken from Takeda et al. (2010).

The $r_0(8542)$ values are plotted in Figure 8 (a) as a function of the amplitude of stellar brightness variation ($\langle \text{BVamp} \rangle$). We calculated $\langle \text{BVamp} \rangle$ listed in Table 1 by taking the average of the amplitude values of Q2~Q16 data. The amplitude value in each Quarter is available in Supplementary Data of this paper. We did not use Q0, Q1, and Q17 data since the duration of these three quarters is short ($\lesssim 30$ days) compared to those of the other 15 quarters (~ 90 days) (Thompson et al. 2013). The errors of $\langle \text{BVamp} \rangle$ in Table 1 correspond to the maximum and minimum of the amplitude values of Q2~Q16 data. The solar $r_0(8542)$ value in Takeda et al. (2010) ($r_0(8542) = 0.193$) is also plotted for reference. The solar brightness variation amplitude in this figure is calculated from the sunspot coverage in the observation date (2007 February 2) of Takeda et al. (2010), and its maximum and minimum value shown here correspond to the typical sunspot coverage of the solar maximum and minimum, respectively. In Figure 8 (a), there is a rough positive correlation between $r_0(8542)$ and $\langle \text{BVamp} \rangle$. Assuming that the brightness variation of superflare stars is caused by the rotation of a star with starspots, the brightness variation amplitude ($\langle \text{BVamp} \rangle$) corresponds to the starspot coverage of these stars. Then, we can say that there is a rough positive correlation between the starspot coverage and chromospheric activity level ($r_0(8542)$). This rough correlation shows us that all the target stars expected to have large starspots on the basis of their large amplitude of the brightness variation show high magnetic activity compared to the Sun. In other words, our assumption that the amplitude of the brightness variation correspond to the spot coverage is supported, since high magnetic activity, which are confirmed by using $r_0(8542)$ values, are considered to be caused by the existence of large starspots.

¹ The dotted line in Figure 5 (a) of Takeda et al. (2010) shows the expected variation of $r_0(8542)$ due to the blurring effect caused by an increase of $v \sin i$ is small compared to the real changes of the stellar activity level. Then we here consider that this effect does not have any essential effects on the interpretation of Figure 7 (b).

In Figure 8 (b), we also plot $\langle fB \rangle$ values that we estimated from $r_0(8542)$ in Section 3.2, as a function of $\langle \text{BVamp} \rangle$. With this figure, we can confirm the same conclusion as we did with Figure 8 (a), though the errors of $\langle fB \rangle$ values are a bit large especially for less active stars. In Appendix 1, we also investigated the emission flux of Ca II IRT and H α lines for reference, and confirmed basically the same conclusions as we did with $r_0(8542)$ index in this section.

In addition to the analyses in this paper, we plan to discuss the Li abundances and stellar age of superflare stars in another future paper (Honda et al. in preparation). As we have introduced previous researches in Section 4.5 of Notsu et al. (2013a), Li abundance can provide some constraints on the age of G-type stars (e.g., Soderblom et al. 1993a; Sestito & Randich 2005). Information of stellar age is important since the stellar activity has a deep relation with the stellar age (e.g., Soderblom et al. 1991), but this point is beyond the scope of this paper.

6. Summary

We have performed high dispersion spectroscopic observations of 50 superflare stars with Subaru/HDS. More than half (34 stars) of these 50 target superflare stars show no evidence of binarity, and we measured stellar parameters of these 34 stars in our previous study (Paper I). In this paper, we investigated whether the quasi-periodic brightness variation of superflare stars is explained by the rotation, and whether superflare stars have large starspots, by using stellar parameters derived in Paper I. First, the value of $v \sin i$ measured from spectroscopic results is consistent with the rotational velocity estimated from the period of the brightness variation. Next, we measured the intensity of Ca II IRT and H α lines, which are good indicators of stellar chromospheric activity, and compared them with other stellar properties. The intensity of Ca II IRT lines indicates that the mean magnetic field strength ($\langle fB \rangle$) of the target superflare stars can be higher than that of the Sun. We found a correlation between the amplitude of the brightness variation and the intensity of Ca II IRT. All the targets expected to have large starspots because of their large amplitude of the brightness variation show high chromospheric activity compared to the Sun. These results support that the brightness variation of superflare stars is explained by the rotation with large starspots.

This study is based on observational data collected with Subaru Telescope, which is operated by the National Astronomical Observatory of Japan. We are grateful to Dr. Akito Tajitsu and other staffs of the Subaru Telescope for making large contributions in carrying out our observations. We would also like to thank Dr. Yoichi Takeda for his many useful advices on the analysis of our Subaru/HDS data, and for his opening the TGVIT and SPTOOL programs into public. When we conducted our solar observation at Hida Observatory mentioned in Section 3.2, we received important advices and kind supports from Dr. Satoru Ueno, Dr. Tetsu Anan, Dr. Reizaburo Kitai, Dr. Ayumi Asai, and other members of Kwasan and Hida Observatories, Kyoto University. Kepler was selected as the tenth Discovery mission. Funding for this mission is provided by the NASA Science Mission Directorate. The Kepler data presented in this paper were obtained from the Multimission Archive at STScI. This work was supported by the Grant-in-Aids from the Ministry of Education, Culture, Sports, Science and Technology of Japan (No. 25287039, 26400231, and 26800096).

References

- Alonso, A., Arribas, S., & Martinez-Roger, C. 1996, *A&A*, 313, 873
- Anderson, R. I., Reiners, A., Solanki, S. K. 2010, *A&A*, 522, A81
- Basri, G., et al. 2011, *AJ*, 141, 20
- Brown, T.M., Latham, D. W., Everett, M. E., & Esquerdo, G. A. 2011, *ApJ*, 142, 112
- Candelaresi, S., Hillier, A., Maehara, H., Brandenburg, A., & Shibata, K. 2014, *ApJ*, 792, 67
- Emslie, et al., 2012, *ApJ*, 759, 71
- Foing, B. H., Crivellari, L., Vladilo, G., Rebolo, R., & Beckman, J. E. 1989, *A&AS*, 80, 189
- Frasca, A., & Catalano, S. 1994, *A&A*, 284, 883
- Frasca, A., Fröhlich, H.-E., Bonanno, A., Catanzaro, G., Biazzo, K., & Molenda-Żakowicz, J. 2011, *A&A*, 532A, 81F
- Gray, D. F. 2005, *The Observation and Analysis of Stellar Photospheres*, 3rd ed. (Cambridge: Cambridge University Press)
- Hall, J.C. 1996, *PASP*, 108, 313
- Hirano, T., Sanchis-Ojeda, R., Takeda, Y., Narita, N., Winn, J. N., Taruya, A., & Suto, Y. 2012, *ApJ*, 756, 66
- Koch, D. G., et al. 2010, *ApJ*, 713, L79
- Lanza, A. F., Rodonò, M., Pagano, I., Barge, P., & Llebaria, A. 2003, *A&A*, 403, 1135
- Linsky, J. L., Hunten, D. M., Sowell, R., Glackin, D. L., & Kelch, W. L. 1979, *ApJS*, 41, 481
- Livingston, W., Wallace, L., White, O. R., & Giampapa, M. S. 2007, *ApJ*, 657, 1137
- Maehara, H., et al. 2012 *Nature*, 485, 478
- Martínez-Arnáiz, R., López-Santiago, J., Crespo-Chacón, I., & Montes, D. 2011, *MNRAS*, 414, 2629
[Erratum: *MNRAS*, 417, 3100]
- Nakai, Y., & Hattori, A. 1985, *Memoirs Faculty of Sciences University of Kyoto*, 36, 385
- Nogami, D., Notsu, Y., Honda, S., Maehara, H., Notsu, S., Shibayama, T., & Shibata, K. 2014, *PASJ*,

- 2014, 66, L4
- Noguchi, K., et al. 2002, PASJ, 54, 855
- Notsu, S., Honda, S., Notsu, Y., Nagao, T., Shibayama, T., Maehara, H., Nogami, D., & Shibata, K. 2013a, PASJ, 65, 112
- Notsu, Y., et al. 2013b ApJ, 771, 127
- Notsu, Y., Honda, S., Maehara, H., Notsu, S., Shibayama, T., Nogami, D., & Shibata, K. 2015, PASJ, in press (Paper I)
- Noyes, R. W., Hartmann, L. W., Baliunas, S. L., Duncan, D. K., & Vaughan, A. H. 1984, ApJ, 279, 763
- Pesnell, W. D., Thompson, B. J., & Chamberlin, P. C. 2012, Sol. Phys., 275, 3
- Priest, E. R. 1981, Solar Flare Magnetohydrodynamics (New York; Gordon and Breach Science Publishers)
- Reinhold, T., Reiners, A., & Basri, G. 2013, A&A, 560, A4
- Schaefer, B. E., King, J. R., & Deliyannis, C. P. 2000, ApJ, 529, 1026
- Scherrer, P. H., et al. 2012, Sol. Phys., 275, 207
- Schou, J., et al. 2012, Sol. Phys., 275, 229
- Schrijver, C. J., Cote, J., Zwaan, C., & Saar, S. H. 1989, ApJ, 337, 964
- Sestito, P., & Randich, S. 2005, A&A, 442, 615
- Shibata, K., & Magara, T. 2011, Living Rev. Sol. Phys, 8, 6
- Shibata, K., et al. 2013, PASJ, 65, 49
- Shibayama, T., et al. 2013, ApJS, 209, 5
- Soderblom, D. R., Duncan, D. K., & Johnson, D. R. H. 1991, ApJ, 375, 722
- Soderblom, D. R., Jones, B. F., Balachandran, S., Stauffer, J. R., Duncan, D. K., Fedele, S. B., & Hudon, J. D. 1993, AJ, 106, 1059
- Soderblom, D. R., Stauffer, J. R., Hudon, J. D., & Jones, B. F. 1993, ApJS, 85, 315
- Takeda, Y., Honda, S., Kawanomoto, S., Ando, H., & Sakurai, T. 2010, A&A, 515, A93
- Thompson, S. E., et al. 2013, Kepler Data Release 23 Notes (KSCI-19063-001)

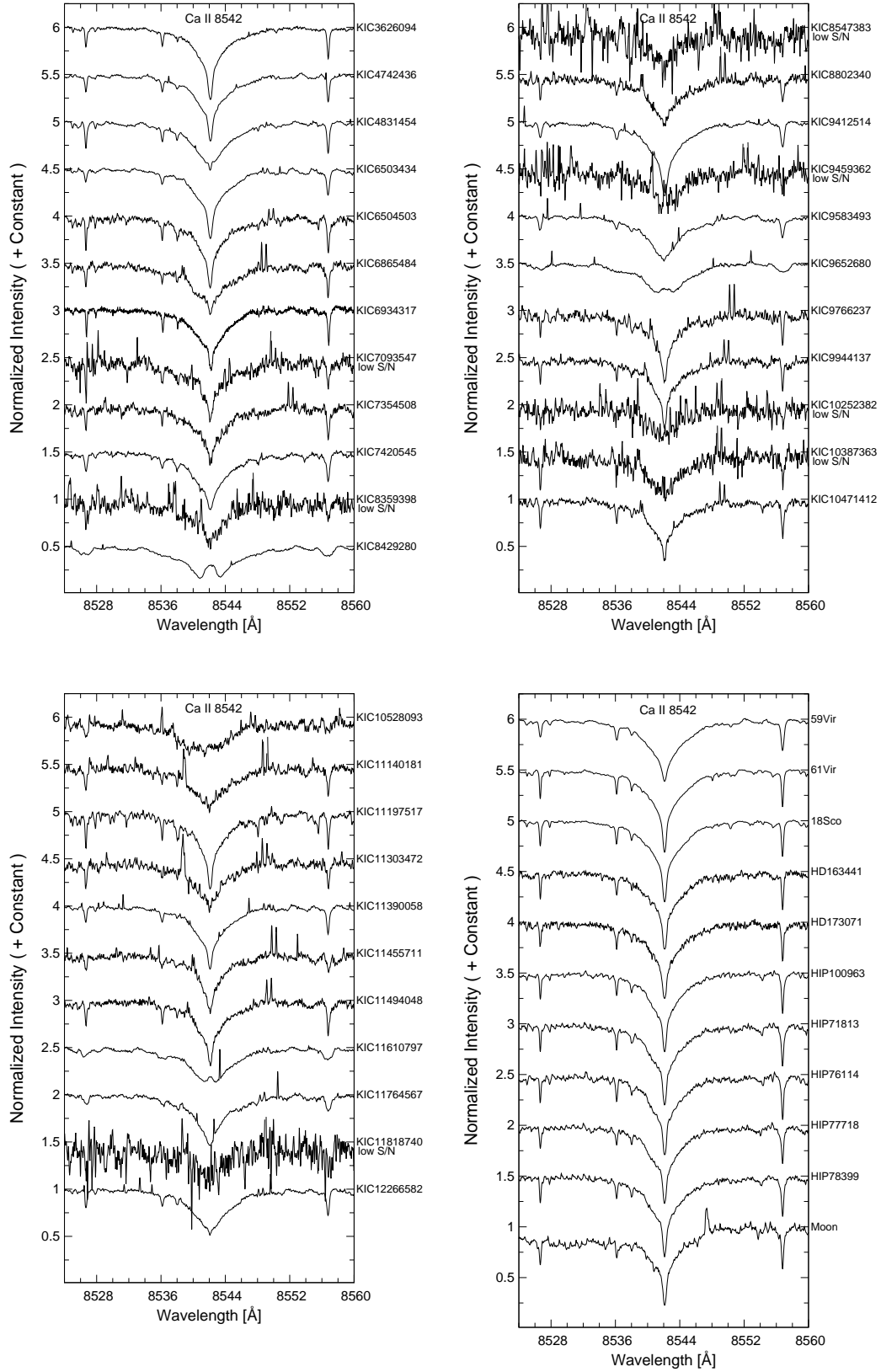


Fig. 1. Spectra around Ca II 8542 line of the 34 superflare stars that show no evidence of binarity, 10 comparison stars, and Moon. The wavelength scale is adjusted to the laboratory frame. Co-added spectra are used here in case that the star was observed multiple times.

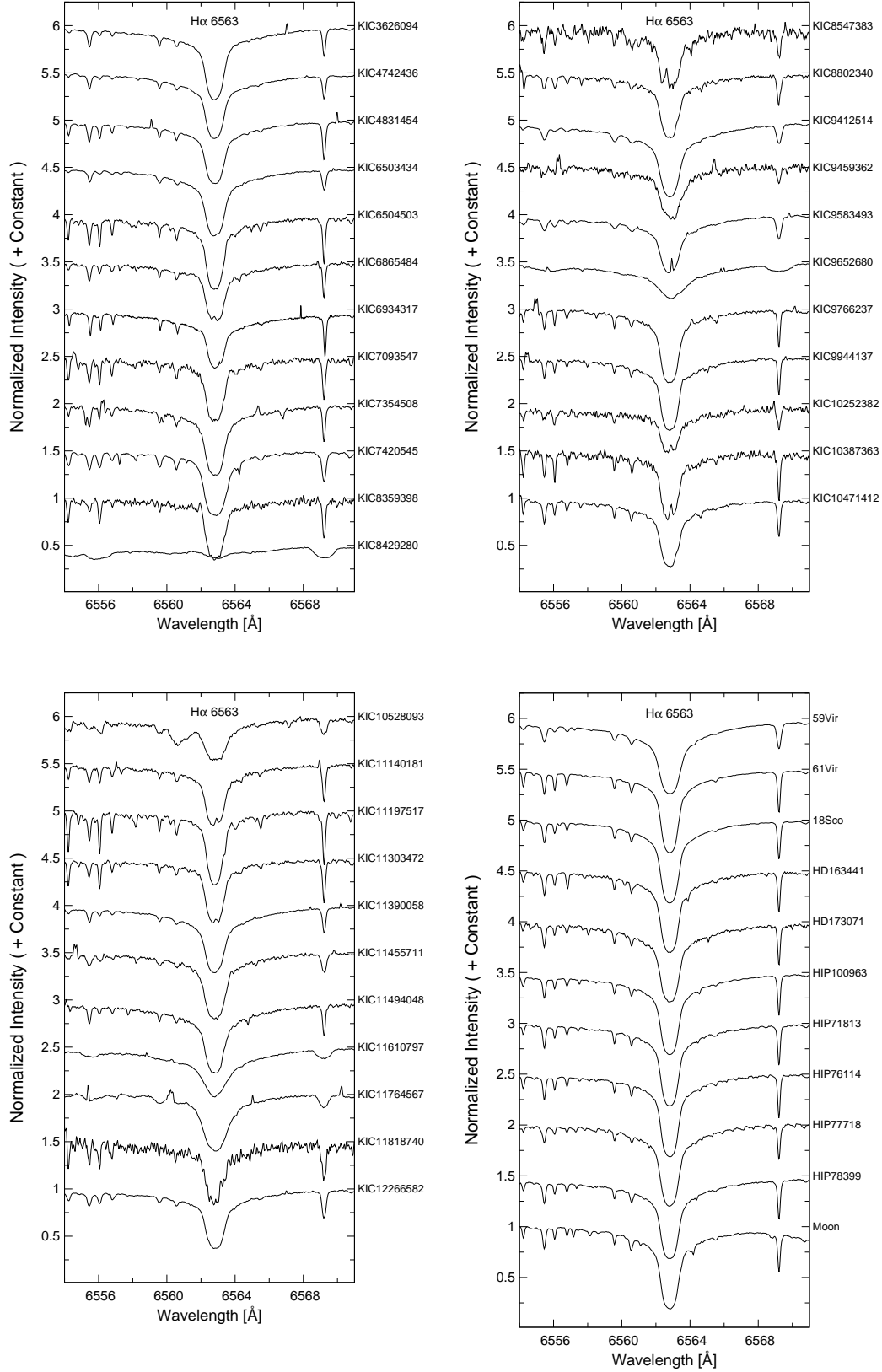


Fig. 2. Spectra around H α 6563 line of the 34 superflare stars that show no evidence of binarity, 10 comparison stars, and Moon. The wavelength scale is adjusted to the laboratory frame. Co-added spectra are used here in case that the star was observed multiple times.

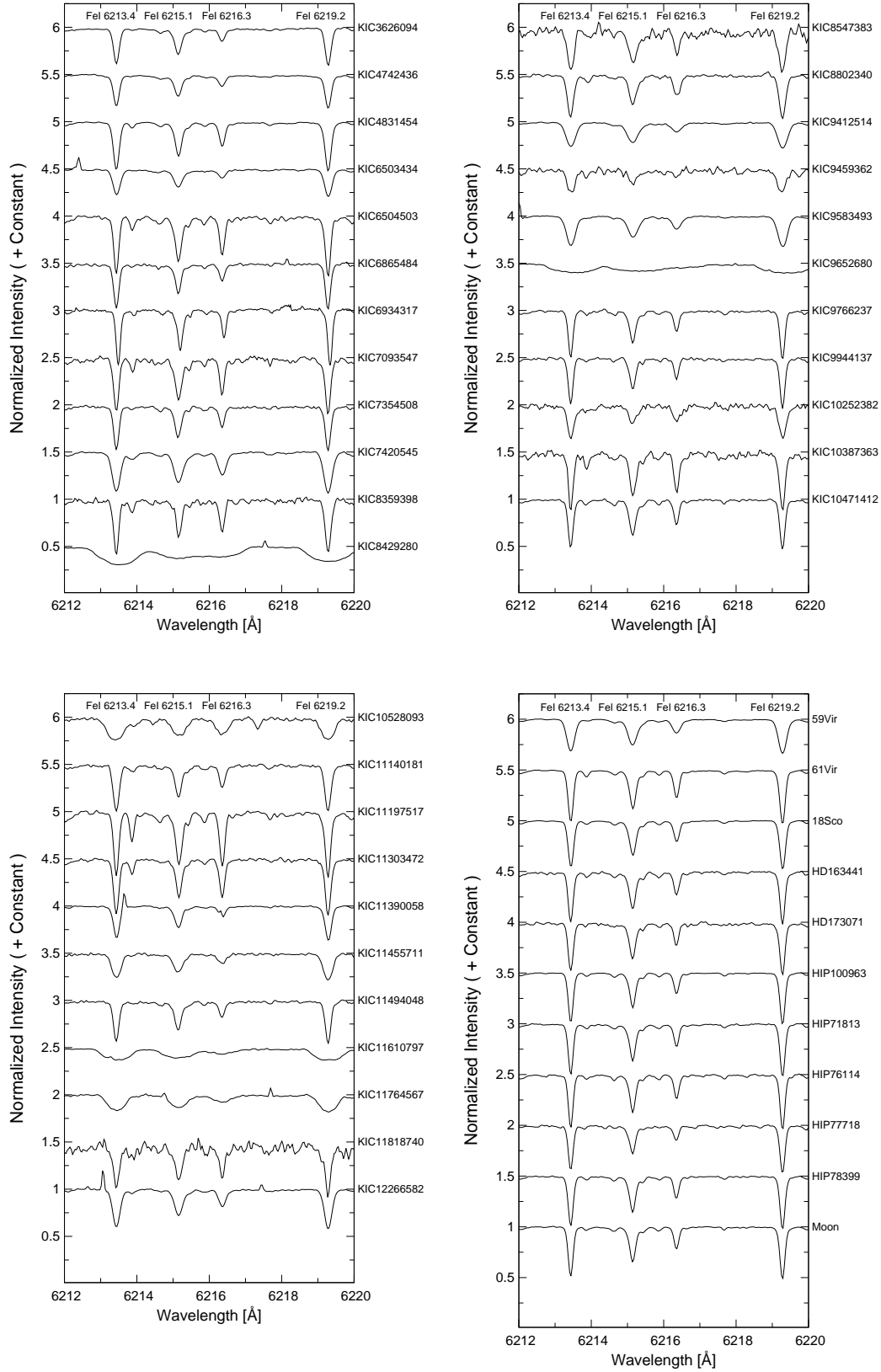


Fig. 3. Example of photospheric absorption lines, including Fe I 6213, 6215, 6216, and 6219, of the 34 superflare stars that show no evidence of binarity, 105 comparison stars, and Moon. The wavelength scale is adjusted to the laboratory frame. Co-added spectra are used here in case that the star was observed multiple times.

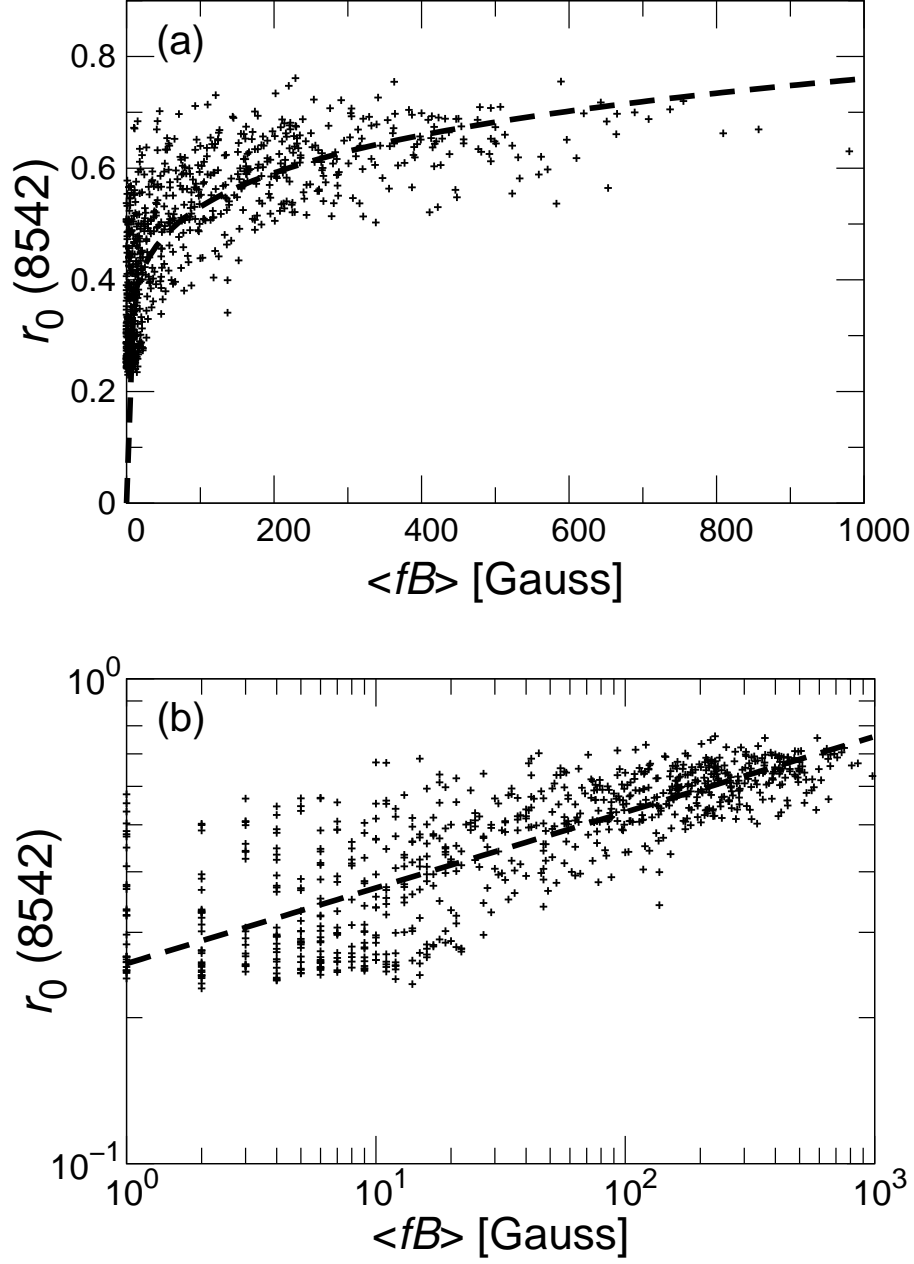


Fig. 4. (a) Residual flux normalized by the continuum level at the core of Ca II 8542 line ($r_0(8542)$ index) vs. the intensity of photospheric magnetic field ($\langle fB \rangle$), on the basis of the data of our solar observation using DST, Hida Observatory. The dashed line corresponds to Equation (1).
(b) Log-log plot of the data shown in (a). The dashed line also corresponds to Equation (1).

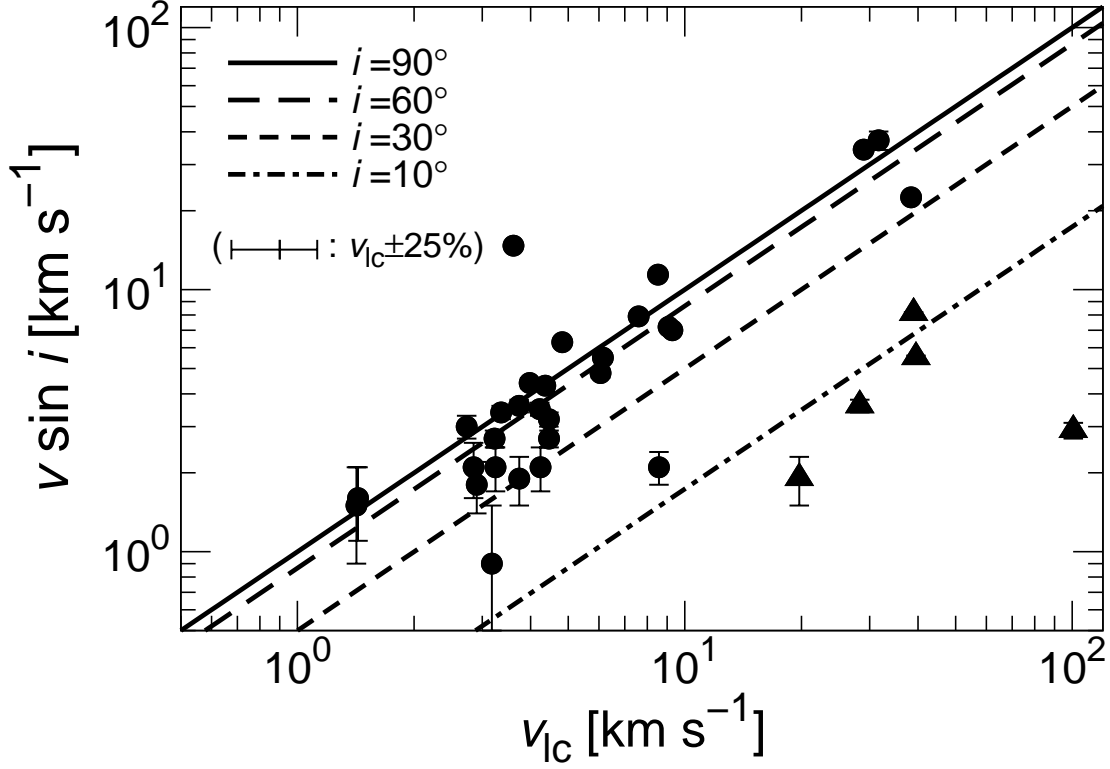


Fig. 5. Projected rotational velocity ($v \sin i$) as a function of the stellar rotational velocity (v_{lc}) estimated from the period of the brightness variation and stellar radius. The typical error of v_{lc} is about $\pm 25\%$ of each value. The error value of $v \sin i$ is listed in Table 4 of Paper I. The solid line represents the case that our line of sight is vertical to the stellar rotation axis ($i = 90^\circ$; $v \sin i = v_{lc}$). We also plot three different lines, which correspond to smaller inclination angles ($i = 60^\circ, 30^\circ, 10^\circ$). Filled triangles represent superflare stars whose inclination angle is especially small ($i \leq 13^\circ$), while filled circles represent the other stars ($i > 13^\circ$).

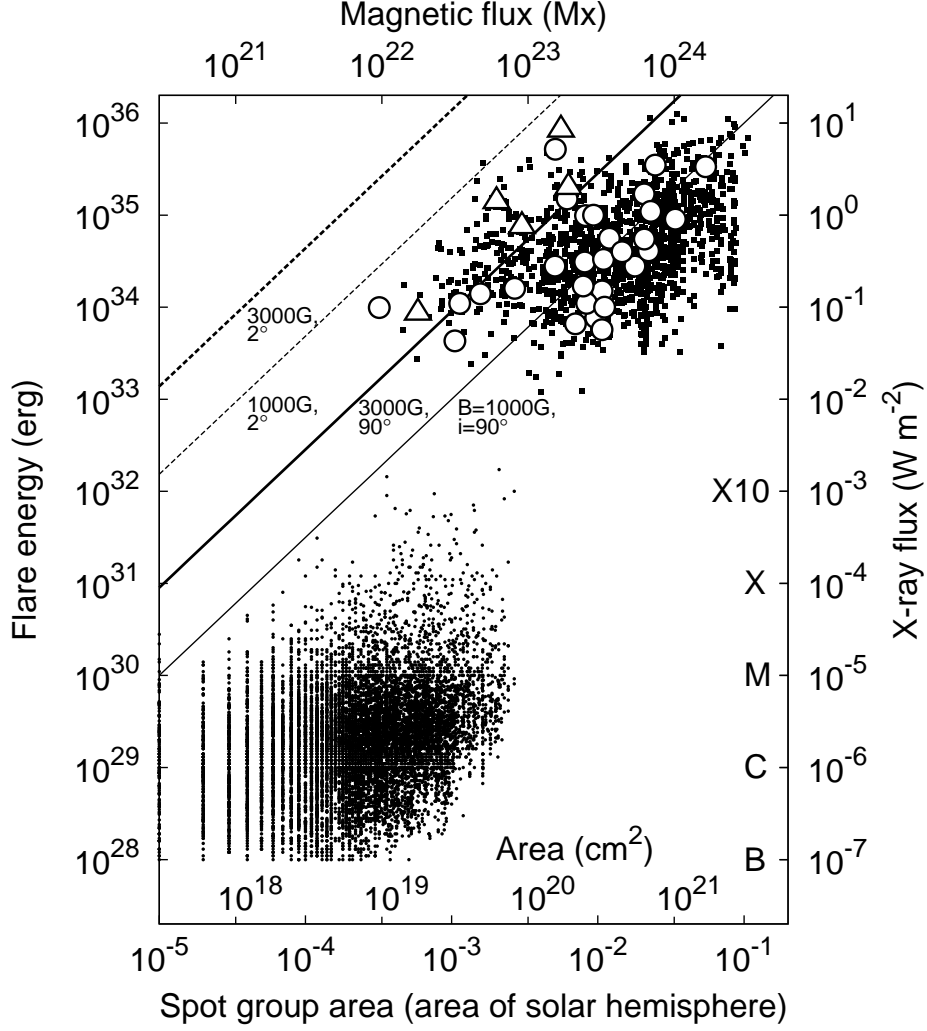


Fig. 6. Scatter plot of the flare energy as a function of the spot coverage. The data of superflares on solar-type stars (filled squares) and solar flares (filled circles) in this figure are completely the same as those in Figure 10 of Notsu et al. (2013b). Thick and thin solid lines corresponds to the analytic relation between the spot coverage and the flare energy, which is obtained from Equation (14) of Notsu et al. (2013b) for $B=3,000\text{G}$ and $1,000\text{G}$. The thick and thin dashed lines correspond to the same relation in case of $i=2^\circ$ (nearly pole-on) for $B=3,000\text{G}$ and $1,000\text{G}$. The right-hand vertical axis (X-ray flux) and the horizontal axis at the top (Magnetic flux) are roughly estimated in the completely same way as done in Figure 10 of Notsu et al. (2013b). Open circle and triangle points on the filled squares represent the data points of the most energetic superflare event reported in Shibayama et al. (2013) of the 34 target superflare stars. Their energy values are listed in 9th column of Table 1 of Paper I. Open triangles represent superflare stars whose inclination angle is especially small ($i \leq 13^\circ$), while open circles represent the others ($i > 13^\circ$). This classification is on the basis of Figure 5.

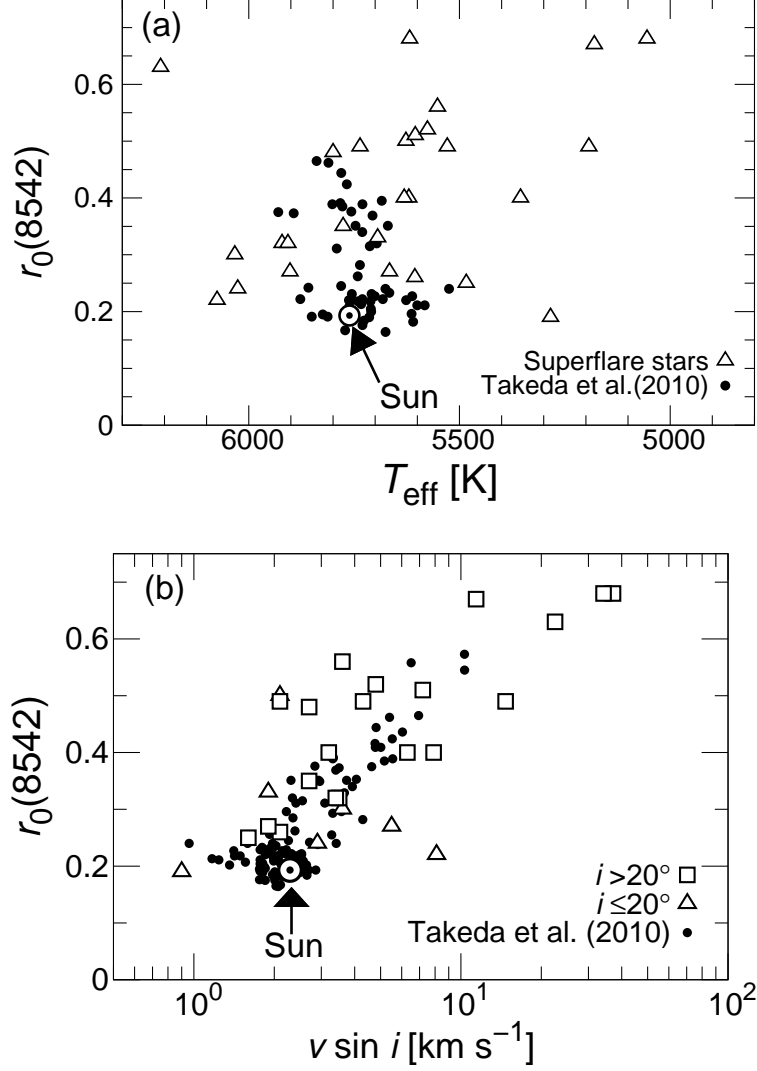


Fig. 7. (a) $r_0(8542)$ as a function of T_{eff} of the stars. In addition to the results of the target superflare stars (open triangles), we also plotted the data of ordinary solar-type stars in Takeda et al. (2010) (black filled circles). The solar $r_0(8542)$ value in Takeda et al. (2010) ($r_0(8542) = 0.193$ and $T_{\text{eff}} = 5761$ K) is also plotted using a circled dot point for reference.

(b) $r_0(8542)$ as a function of $v \sin i$. The results of the target superflare stars are plotted, being classified into two groups on the basis of stellar inclination angles (i) estimated in Section 4. Open squares represent superflare stars with $i > 20^\circ$, while open triangles represent those with $i \leq 20^\circ$. The data of ordinary solar-type stars reported in Takeda et al. (2010) are plotted by using black circle points. The solar $r_0(8542)$ and $v \sin i$ value in Takeda et al. (2010) ($r_0(8542) = 0.193$ and $v \sin i = 2.29$ km s $^{-1}$) is also plotted by using a circled dot point for reference.

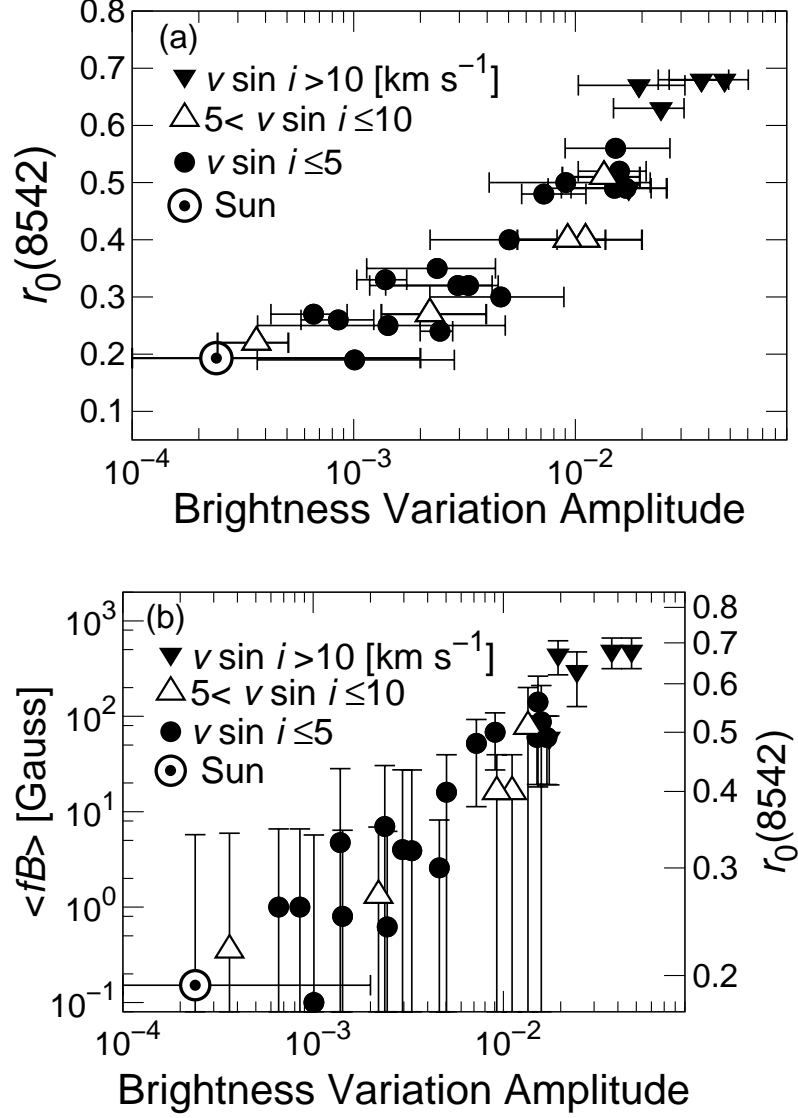


Fig. 8. (a) $r_0(8542)$ as a function of the amplitude of stellar brightness variation that are listed as $\langle \text{BVamp} \rangle$ in Table 1. The results of the target superflare stars are plotted, being classified into three groups on the basis projected rotational velocity. Black filled inverted triangles represent superflare stars with $v \sin i > 10$ km s $^{-1}$, open regular triangles represent those with $5 < v \sin i \leq 10$ km s $^{-1}$, and filled circles represent those with $v \sin i \leq 5$ km s $^{-1}$. The solar value is plotted by using a circled dot point. (b) $\langle fB \rangle$ as a function of amplitude of stellar brightness variation. The results of the target superflare stars are plotted, being classified into three groups using the same symbols as in (a). The errorbars of $\langle \text{BVamp} \rangle$ are not plotted here since it is hard to see if vertical and horizontal error bars are both plotted. The $r_0(8542)$ values shown on the right-hand vertical axis correspond to $\langle fB \rangle$ on the left-hand vertical axis on the basis of Equation (1). The solar value is also plotted by using a circled dot point.

Table 1. Rotational velocity and activity index of Ca II IRT and H α .

Starname	$v \sin i$ [km s ⁻¹]	v_{lc} [km s ⁻¹]	P_0^a [day]	$\langle BVamp \rangle^b$ [%]	$r_0(8542)$	$\langle fB \rangle^c$ [Gauss]	$r_0(8498)$	$r_0(8662)$	$r_0(H\alpha)$
KIC3626094	2.9	100.6	0.7	$0.24^{+0.03}_{-0.05}$	0.24	0.6 ± 6	0.33	0.25	0.21
KIC4742436	3.6	28.3	2.3	$0.46^{+0.43}_{-0.24}$	0.30	3 ± 6	0.40	0.32	0.29
KIC4831454	2.1	8.6	5.2	$0.91^{+1.27}_{-0.50}$	0.50	68 ± 41	0.58	0.44	0.32
KIC6503434	5.5	39.5	3.9	$0.22^{+0.18}_{-0.09}$	0.27	1 ± 6	0.35	0.27	0.27
KIC6504503	1.6	1.4	31.8	$0.14^{+0.34}_{-0.11}$	0.25	0.8 ± 6	0.35	0.26	0.21
KIC6865484	2.7	4.5	10.3	$0.72^{+0.40}_{-0.15}$	0.48	52 ± 41	0.56	0.42	0.40
KIC6934317	1.9 ^d	19.7	2.5	$0.14^{+0.03}_{-0.04}$	0.33 ^d	5 ± 24	0.43 ^d	0.37 ^d	0.42 ^d
KIC7093547 ^e	2.1	3.2	14.2	$0.37^{+0.32}_{-0.19}$	-	-	-	-	0.32
KIC7354508	3.2	4.5	16.8	$0.50^{+0.32}_{-0.28}$	0.40	16 ± 24	0.42	0.33	0.24
KIC7420545	6.3	4.8	36.2	$1.11^{+0.89}_{-0.56}$	0.40	16 ± 24	0.50	0.37	0.32
KIC8359398 ^e	1.8	2.9	12.7	$1.68^{+0.56}_{-0.96}$	-	-	-	-	0.34
KIC8429280	37.1	31.6	1.2	$3.71^{+1.21}_{-1.34}$	0.68	489 ± 173	0.80	0.72	0.93
KIC8547383 ^e	4.4	4.0	14.8	$0.66^{+0.38}_{-0.31}$	-	-	-	-	0.38
KIC8802340	4.3	4.4	10.3	$1.69^{+0.88}_{-0.83}$	0.49	60 ± 41	0.57	0.46	0.31
KIC9412514	8.1	38.9	3.7	$0.04^{+0.01}_{-0.01}$	0.22	0.4 ± 6	0.32	0.22	0.19
KIC9459362 ^e	7.0	9.3	12.6	$1.78^{+1.22}_{-0.88}$	-	-	-	-	0.46
KIC9583493	7.2	9.1	5.5	$1.35^{+0.61}_{-0.47}$	0.51	77 ± 123	0.61	0.49	0.38
KIC9652680	34.2	29.0	1.5	$4.72^{+1.32}_{-2.06}$	0.68	489 ± 173	0.76	0.69	0.60
KIC9766237	2.1 ^f	4.2	14.2	$0.09^{+0.04}_{-0.03}$	0.26 ^f	1 ± 6	0.40	0.28	0.23
KIC9944137	1.9 ^f	3.7	12.6	$0.07^{+0.03}_{-0.02}$	0.27 ^f	1 ± 6	0.41	0.29	0.22
KIC10252382 ^e	5.5	6.1	16.8	$2.93^{+3.95}_{-1.63}$	-	-	-	-	0.52
KIC10387363 ^e	1.5	1.4	29.9	$0.30^{+0.35}_{-0.18}$	-	-	-	-	0.31
KIC10471412	2.7	3.2	15.2	$0.24^{+0.20}_{-0.12}$	0.35	7 ± 24	0.48	0.34	0.28
KIC10528093	11.4	8.5	12.2	$1.94^{+1.19}_{-0.90}$	0.67	445 ± 173	0.75	0.66	0.51
KIC11140181	3.6	3.7	11.5	$1.52^{+1.15}_{-0.62}$	0.56	141 ± 123	0.63	0.45	0.36
KIC11197517	0.9	3.2	14.3	$0.10^{+0.18}_{-0.06}$	0.19	0.1 ± 6	0.27	0.21	0.22
KIC11303472	2.1	2.8	13.5	$1.50^{+0.69}_{-0.75}$	0.49	60 ± 41	0.56	0.39	0.33
KIC11390058	3.5	4.2	12.0	$0.33^{+0.12}_{-0.21}$	0.32	4 ± 24	0.42	0.30	0.29
KIC11455711	7.9	7.6	13.9	$0.92^{+0.44}_{-0.42}$	0.40	16 ± 24	0.59	0.44	0.30
KIC11494048	3.4	3.4	14.8	$0.30^{+0.13}_{-0.16}$	0.32	4 ± 24	0.45	0.31	0.23
KIC11610797	22.5	38.4	1.6	$2.44^{+0.66}_{-0.95}$	0.63	300 ± 173	0.70	0.61	0.46
KIC11764567	14.7	3.6	22.4	$1.74^{+0.85}_{-0.78}$	0.49	60 ± 41	0.57	0.44	0.39
KIC11818740 ^e	3.0	2.7	15.4	$1.40^{+0.81}_{-0.93}$	-	-	-	-	0.35
KIC12266582	4.8	6.1	6.9	$1.58^{+0.50}_{-0.55}$	0.52	88 ± 123	0.61	0.48	0.37

Table 1. (Continued)

Starname	$v \sin i$	v_{lc}	P_0^a	$\langle BVamp \rangle^b$	$r_0(8542)$	$\langle fB \rangle^c$	$r_0(8498)$	$r_0(8662)$	$r_0(H\alpha)$
	[km s ⁻¹]	[km s ⁻¹]	[day]	[%]		[Gauss]			
59Vir	6.1	-	-	-	0.40	16±24	0.50	0.38	0.27
61Vir	<1.0	-	-	-	0.19	0.1±6	0.30	0.20	0.18
18Sco	2.0	-	-	-	0.20	0.2±6	0.30	0.21	0.18
HD163441	2.5	-	-	-	0.23	0.5±6	0.34	0.25	0.19
HD173071	2.7	-	-	-	0.25	0.8±6	0.34	0.25	0.21
HIP100963	2.4	-	-	-	0.22	0.4±6	0.34	0.22	0.20
HIP71813	2.3	-	-	-	0.20	0.2±6	0.30	0.20	0.19
HIP76114	1.8	-	-	-	0.21	0.3±6	0.32	0.20	0.19
HIP77718	2.5	-	-	-	0.23	0.5±6	0.34	0.23	0.20
HIP78399	2.5	-	-	-	0.21	0.3±6	0.32	0.21	0.18
Moon	2.4	-	-	-	0.20	0.2±6	0.33	0.22	0.19

^a Period values estimated from the Kepler data (Quarter 2~16 data), which are reported in Paper I.

^b The amplitude of the brightness variation. This value is calculated by taking the average of the amplitude value of each Quarter (Q2~Q16) data. (The amplitude value of each Quarter data is available in Supplementary Data.) The errors of $\langle BVamp \rangle$ correspond to the maximum and minimum of the amplitude value of all Quarter (Q2~Q16) data.

^c Mean intensity of the stellar magnetic field estimated from $r_0(8542)$ index (See Section 3.2 for details.).

^d We already reported the values of KIC6934317 in Notsu et al. (2013a).

^e We do not use Ca II IRT (8498/8542/8662) data of these stars (KIC7093547, KIC8359398, KIC8547383, KIC9459362, KIC10252382, KIC10387363, and KIC11818740) since S/N ratio of the observed spectra is too low.

^f We already reported the $v \sin i$ and $r_0(8542)$ values of KIC9766237 and KIC9944137 in Nogami et al. (2014).

Appendix 1. Discussion of chromospheric activities using “Flux Method”.

We measured the values of the r_0 of Ca II IRT and H α in Section 3.1, and discussed chromospheric activity of superflare stars by using the $r_0(8542)$ index in Section 5. This index is an indicator of chromospheric activity as described in the above sections, but it also depends on $v \sin i$ (e.g., Figure 5(a) of Takeda et al. 2010). A large value of $v \sin i$ can indeed increase the residual flux, mimicking the effect of filling the line core with chromospheric emission. Because of this, we here roughly estimated the emission flux of the Ca II 8542 and H α lines in order to remove this influence of $v \sin i$. The ways of estimation is basically the same as done in Notsu et al. (2013a), and we summarize the method in the following.

We used the spectral subtraction technique (e.g., Frasca & Catalano 1994; Frasca et al. 2011; Martínez-Arnáiz et al. 2011). With this subtraction process, we can subtract the underlying photospheric contribution from the spectrum of the star, and can investigate the spectral emission originating from the chromosphere in detail (Martínez-Arnáiz et al. 2011). We used the spectrum of 61Vir obtained in this observation as an inactive template to be subtracted from the spectrum of the target stars. This is because 61Vir is a slowly rotating and non-active early G-type main sequence star (e.g., Anderson et al. 2010). We measured the excess equivalent width (W_λ^{em}) of the Ca II 8542 and H α lines by using the residual spectrum around the line core resulting from this subtraction process. We then derived emission fluxes (F_λ^{em}) of Ca II 8542 and H α lines from W_λ^{em} of these lines by the following relation, $F_\lambda^{\text{em}} = W_\lambda^{\text{em}} F_\lambda^{\text{cont}}$ (Martínez-Arnáiz et al. (2011)), where F_λ^{cont} is the continuum flux around the wavelength of each line. We calculated F_λ^{cont} by using the the following empirical relationships between F_λ^{cont} and color index ($B - V$) derived by Hall (1996):

$$\log F_{\text{H}\alpha}^{\text{cont}} = [7.538 - 1.081(B - V)] \pm 0.033, \quad +0.0 \leq B - V \leq +1.4, \quad (\text{A1})$$

$$\log F_{\text{IRT}}^{\text{cont}} = [7.223 - 1.330(B - V)] \pm 0.043, \quad -0.1 \leq B - V \leq +0.22, \quad (\text{A2})$$

$$\log F_{\text{IRT}}^{\text{cont}} = [7.083 - 0.685(B - V)] \pm 0.055, \quad +0.22 \leq B - V \leq +1.4. \quad (\text{A3})$$

For deriving $B - V$ values, we used the following empirical relations of low-mass main-sequence stars (F0V-K5V) among $B - V$, T_{eff} , and $[\text{Fe}/\text{H}]$ derived by Alonso et al. (1996):

$$(B - V) = -0.9837 + 1.8652\theta_{\text{eff}} - 0.0324\theta_{\text{eff}}^2 + 0.1293\theta_{\text{eff}}[\text{Fe}/\text{H}] - 0.0085[\text{Fe}/\text{H}] + 0.0199[\text{Fe}/\text{H}]^2, \quad \sigma(B - V) = 0.039\text{mag}, \quad (\text{A4})$$

where $\theta_{\text{eff}} = 5040/T_{\text{eff}}$.

The estimated values of the emission flux of Ca II 8542 (F_{8542}^{em}) and H α ($F_{\text{H}\alpha}^{\text{em}}$) are listed in Supplementary Table 1 of this paper. The excess equivalent width values (W_{8542}^{em} and $W_{\text{H}\alpha}^{\text{em}}$) are also listed in this table. As we have already mentioned in Section 3.1, we did not use

the values of Ca II 8542 of 7 target superflare stars (KIC7093547, KIC8359398, KIC8547383, KIC9459362, KIC10252382, KIC10387363, and KIC11818740), which are marked in the 8th column of Supplementary Table 1. This is because the exposure time for such stars was not sufficient and the resultant S/N ratio around Ca II triplet lines is low.

In Figure 9, the F_{8542}^{em} and $F_{\text{H}\alpha}^{\text{em}}$ are plotted as a function of $r_0(8542)$ and $r_0(\text{H}\alpha)$, respectively. The error values of F_{8542}^{em} and $F_{\text{H}\alpha}^{\text{em}}$ in Figure 9 are plotted in the following method. Roughly assuming the upper limit of subtraction error, we here consider the typical error value of the emission flux (F^{em}) is roughly $\pm 50\%$, if excess equivalent width (W^{em}) is larger than $30\text{m}\text{\AA}$ (sufficiently high compared to 61Vir). On the other hand, if the excess equivalent width (W^{em}) is less than $30\text{m}\text{\AA}$ (not so high compared to 61Vir), we consider that the typical error value of the emission flux (F^{em}) is about $\pm 100\%$. We can see a positive correlation between emission flux and r_0 index in this figure, and all of the superflare stars with high $r_0(8542)$ and $r_0(\text{H}\alpha)$ values show high F_{8542}^{em} and $F_{\text{H}\alpha}^{\text{em}}$ values. This positive correlation show us that by using values of the emission flux, we can conclude the basically same conclusions as we did with $r_0(8542)$ index in Section 5.

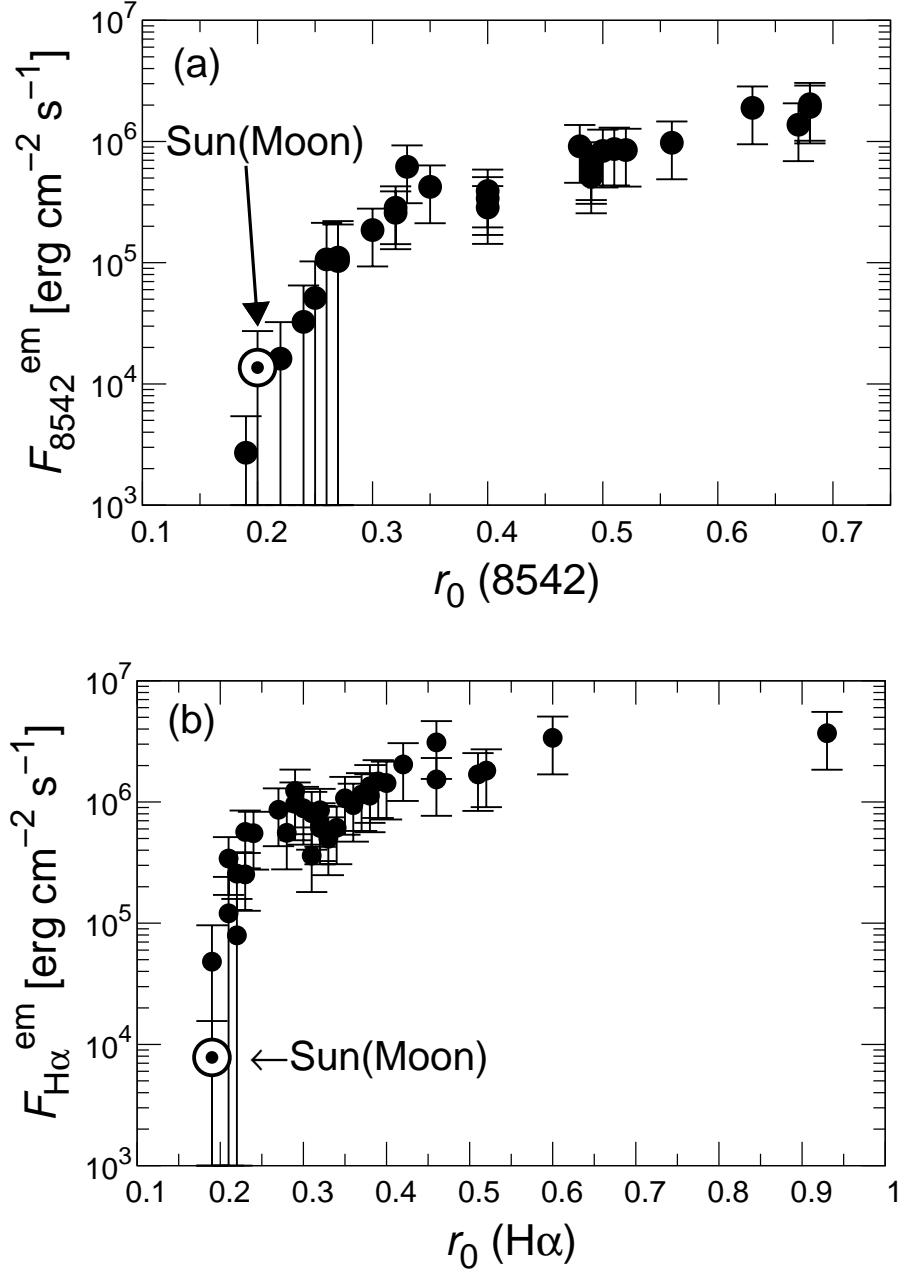


Fig. 9. (a) F_{8542}^{em} as a function of $r_0(8542)$.

(b) $F_{H\alpha}^{\text{em}}$ as a function of $r_0(H\alpha)$.

The Moon value in this paper is also plotted as a solar value for reference with a circled dot in both (a) and (b).